LA-UR-03-03420

Active Sensing using Impedance-Based ARX Models and Extreme Value Statistics for Damage Detection

Timothy R. Fasel, Hoon Sohn, Gyuhae Park, and Charles R. Farrar

Engineering Sciences & Applications Division, Weapon Response Group, M/S T006

Los Alamos National Laboratory, Los Alamos, NM 87545

ABSTRACT

In this paper, the applicability of an auto-regressive model with exogenous inputs (ARX) in the frequency domain to structural health monitoring (SHM) is established. Damage sensitive features that explicitly consider nonlinear system input/output relationships are extracted from the ARX model. Furthermore, because of the non-Gaussian nature of the extracted features, Extreme Value Statistics (EVS) is employed to develop a robust damage classifier. EVS provides superior performance to standard statistical methods because the data of interest are in the tails (extremes) of the damage sensitive feature distribution. The suitability of the ARX model, combined with EVS, to nonlinear damage detection is demonstrated using vibration data obtained from a laboratory experiment of a three-story building model. It is found that the vibration-based method, while able to discern when damage is present in the structure, is unable to localize the damage to a particular joint. An impedance-based active sensing method using piezoelectric (PZT) material as both an actuator and a sensor is then investigated as an alternative solution to the problem of damage localization.

1. INTRODUCTION

Many aerospace, civil, and mechanical systems continue to be used despite aging and the potential for damage accumulation and unpredicted failure. The 1994 Northridge earthquake showed that steel moment-resisting frame structures are susceptible to brittle joint failure [1]. During this earthquake, over 70% of steel frame buildings in Northridge suffered from some form of damage at moment-resisting joints. However, many of the damaged joints remained undetected until one was accidentally found. The cost of visually inspecting a single joint, by removing the architectural cladding and fire retardant, was approximately $10,000. There are currently many nondestructive evaluation (NDE) techniques for identifying damage in structures. However, these NDE methods are based on costly visual procedures or localized experimental methods such as acoustic or ultrasonic methods, magnetic field methods, radiograph, eddy-current methods and thermal field methods. These approaches are limited in usage, as the vicinity of the damage must be known *a priori* and easily accessible. For a more complete literature review of current NDE methods, consult

[2]. If a damage detection method using sensors embedded in a structure can be developed, it would constitute a more economical and quantifiable technique than is currently available. Such a damage identification scheme can potentially provide significant life-safety benefits by preventing unforeseen catastrophic failures.

In recent years, vibration-based damage detection techniques have come to the foreground as a legitimate method to determine structural damage [3,4]. Many previous studies in the literature review focus on identifying damage using linear characteristics. Because damage to a structure will often result in some nonlinear behavior, a damage detection scheme that seeks to use nonlinear characteristics to identify damage could be of great use. The focus of this study is to demonstrate the feasibility of using a frequency domain auto-regressive model with exogenous inputs (ARX) for detecting joint damage in steel moment-resisting frame structures, explicitly considering nonlinear response characteristics. This approach uses coefficients from an ARX frequency domain model originally proposed by Adams and Allemang [5] as the damage sensitive features. These features are then analyzed using a statistical method known as extreme value statistics (EVS).

An impedance-based method using piezoelectric (PZT) patches as both actuators and sensors has also been proven a very powerful tool for structural health monitoring (SHM) [6]. This active sensing method is investigated, with the frequency domain ARX model and EVS, to address limitations in the vibration-based technique. The high frequency range generally used for the impedance-based method (> 30 kHz) is particularly advantageous with regards to damage localization and insensitivity to operational variation. The approach taken in this study is unique in that it uses nonlinear analysis, as opposed to the linear techniques currently employed, to identify damage within the structure. In addition, the inclusion of EVS into the damage detection scheme places the process in a rigorous statistical framework that improves the robustness of the damage classifier.

This paper is organized in the following way. Section 2 introduces the vibration-based damage detection method. In this section, the test structure, the basic four-part SHM process, and EVS are discussed. Results and deficiencies of the vibration-based method are also explained. Section 3 applies the frequency domain ARX model to an impedance-based method and gives results. Section 4 summarizes this paper and discusses future work.

2. VIBRATION-BASED METHOD

2.1 Experimental Setup

The test structure shown in Figures 1, 2 and 3 is an idealized three-story frame structure in a seismic region, constructed of unistrut columns and aluminum floor plates. Support brackets for the columns are bolted to a 3.8-cm-thick aluminum base plate. Floors are 1.3-cm-thick aluminum plates with two-bolt connections to brackets on the unistrut columns. All bolted connections are tightened to a preload of 25 N-m in the undamaged state. Four Firestone airmount isolators, which allow the structure to move freely in horizontal directions, are connected to the bottom of the base plate. The isolators are mounted on aluminum blocks and plywood so that the base of the structure is level with the shaker. The isolators are inflated to 69 kPag. The shaker is connected to the structure by a 15-cm-long, 0.5-cm diameter stinger connected to a tapped hole at the mid-height of the base plate. The shaker is attached 10-cm from the corner on the 46-cm side of the structure, so that both translational and torsional modes can be excited simultaneously. The base excitation is used to simulate various inputs to a building, including ground excitation that is produced by an earthquake. The readers are referred to [7] for more details on the experimental setup.

In this experiment, damage is simulated through reduction of the preload applied by two bolts at the joints of the structure. Multiple damage levels are tested so that the sensitivity of the damage detection method can be investigated. The first damage level is simulated by loosening bolts at the damaged joint from 25 N-m to 1.8 N-m. The large reduction in preload is necessary to allow relative motion between the plate and the column. The next level has the preload being reduced to 0.6 N-m. For the final damage level, bolts on the damaged

joint are completely removed to simulate a crack in the joint. The robustness of the damage detection scheme to multiple damage locations is also investigated. For a summary of damage levels and locations, see Table 1.

bookshelf.jpg (788x1280x16M jpeg)

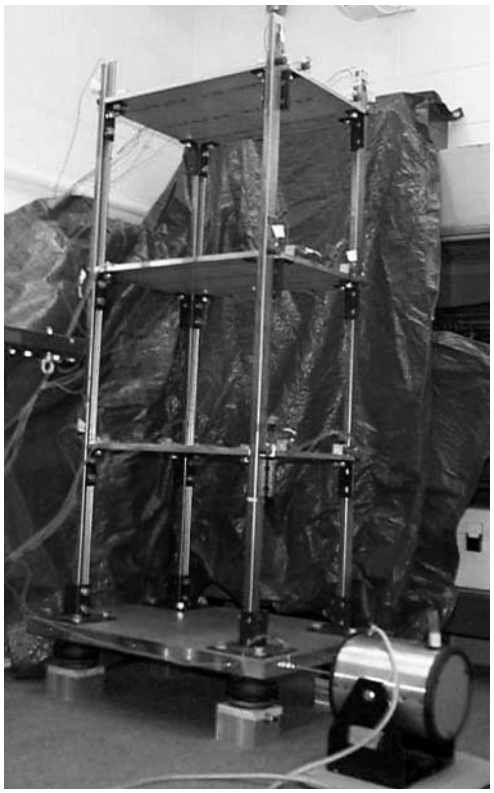

Figure 1: Assembled moment-resisting frame test structure including attached electro-dynamic shaker

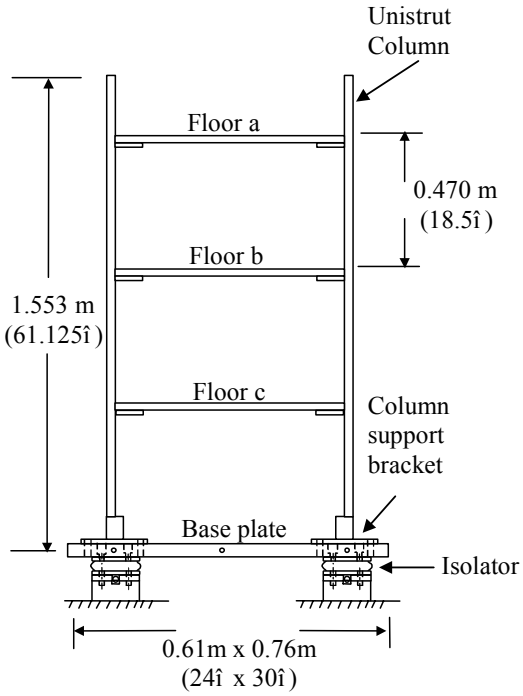

Figure 2: A side view of the test structure

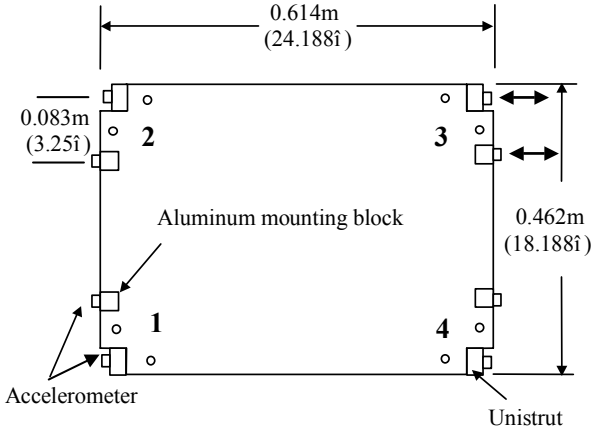

Figure 3: A top view of the assembled test structure

Table 1: Summary of damage levels and locations

Damage Level 1	Bolt preloads reduced from 25 N-m to 1.8 N-m
Damage Level 2	Bolt preloads reduced from 25 N-m to 0.6 N-m
Damage Level 3	Bolts completely removed
Damage Location 1	Joint 2a has induced damage*
Damage Location 2	Joint 4b has induced damage*

* All 3 damage levels are used

An electro-dynamic shaker attached to the base of the structure applies the vibration input. The input excitation is a random waveform with uniform energy content at a frequency range of 0 to 200 Hz. However, it is possible that the shaker dynamics had altered the actual energy content exerted into the structure. This frequency range is higher than normal earthquake engineering applications because a rigorous similitude analysis was not performed on the test structure. Previous experience leads the authors to believe that this frequency range is approximately equivalent to the frequency range of base excitation experienced by a real structure during an earthquake. For example, the first bending mode of the structure is approximately 14 Hz as compared to a first bending mode of approximately 1 Hz on a real structure [8]. Two different base excitation levels are used in the experiment by changing the voltage supplied to the amplifier that powers the shaker. The root mean square (RMS) value of the high excitation level is 1 V, and that of the low excitation level is 0.25 V.

2.2 Structural Health Monitoring

The aforementioned test structure is analyzed using a damage detection process that is the focus of this study. SHM consists of the following four-part process based on a statistical pattern recognition paradigm [9]: Operational Evaluation, Data Acquisition, Feature Extraction and Statistical Model Development.

1) Operational Evaluation

Operational evaluation determines the conditions under which the system to be monitored functions. The first step in this assessment is to define and, to the extent possible, quantify the damage that is to be detected.

Limitations on types of data that can be gathered for use during the damage detection process are also strictly defined during this stage. Because the test structure is located in a controlled laboratory environment, many of the evaluation problems that plague real world applications are not present. For instance, many real world structures are too large to be sufficiently excited using a shaker or impact hammer. In these cases, only ambient vibration can be used to evaluate the condition of the building, which substantially hampers the potential effectiveness of SHM methods. Ambient vibration is typically nonstationary and puts energy in a low frequency range. Dynamic responses in these low frequency ranges are insensitive to local damage. In addition, the exact input to the structure is hard to measure when using ambient vibration for excitation. Ideally, measurements from the building in a known undamaged state will be available. Unfortunately, this situation is not always possible for existing structures. In such a case, SHM can only seek to identify further degradation of structural integrity and cannot discover damage that already exists.

In this study, varying levels of shaker input were used to introduce operational and environmental variability. The damage detection scheme should be able to distinguish between the varying excitation levels and structural damage. This distinction between operational and environmental variations and structural damage is accomplished through a procedure known as data normalization. One essential part of this data normalization process is the following data standardization technique:

$$\bar{\mathbf{x}} = \frac{\mathbf{x} - \mu}{\sigma} \qquad \textbf{(1)}$$

where $\mathbf{x}$ is the original data, $\bar{\mathbf{x}}$ is the standardized data, μ is the mean of the original data, and σ is the standard deviation of the original data. This technique is used so the amplitude of accelerometer response between varying levels of shaker input can be normalized and all signals have zero means.

2) Data Acquisition

Data acquisition in a SHM process begins with the selection of the types of sensors to be used, placement and number of sensors, and the hardware used to transmit the data from the sensors into storage. Intervals at which data are taken must be explored, as the amount of data necessary depends on the specific structure as well as the type of damage to be detected.

The test structure presented in this paper is instrumented with 24 PCB 336C piezoelectric accelerometers. 2 accelerometers that measure horizontal acceleration are placed at each joint, with one accelerometer attached to the plate and the other accelerometer attached to the unistrut column (the exact direction of the acceleration measurement is shown for joint 3 in Figure 3). Each accelerometer is labeled with its own corresponding channel in the data acquisition system. Joints are labeled according to their respective locations on the structure. Each corner is given a number (1-4) and each floor is given a letter (a-c) with (a) being the top floor of the structure and (c) the first floor. This labeling system is illustrated in Figures 2 and 3. The accelerometers are mounted on blocks glued to the floors and unistrut columns. This configuration allows relative motion between the column and the floor to be detected. The nominal sensitivity of each accelerometer is 1 V/g. A commercial data acquisition system controlled from a laptop PC is used to digitize the analog accelerometer signals.

For this study, 8-second time histories are sampled at a rate of 512 Hz, producing 4096 time points in a particular record. A matrix of baseline undamaged data sets is recorded before damage is introduced to the structure. The summary of damage cases is shown in Table 1. For each damage case and base excitation level, three separate time histories are recorded. Before acquiring each data set, the pressure in the airmounts is inspected, the bolt torques throughout the structure are verified, and the accelerometers are inspected for proper mounting.

3) Feature Extraction

Feature extraction involves the selection of certain information from the data that distinguishes between a damaged and an undamaged structure. This extraction often involves condensation of the large amount of available data into a much smaller data set that can be better analyzed in a statistical manner.

The features that are analyzed in this study are drawn from frequency domain analysis of the time histories obtained during experimentation on the test structure. Frequency response is important in structural dynamics because it relates inputs and outputs of the structure at various frequencies. Analyzing these responses can lead to useful information regarding the health of the structure. Conventional frequency response function estimators are based on a linearity assumption for the system. Though global behaviors of many large-scale buildings can be approximated in a linear fashion, there are always local nonlinearities within the structures. Damage to a joint in a building may produce nonlinearity, and any method that seeks to identify the damage location and severity will be enhanced by taking into account this nonlinear behavior. To explicitly consider this nonlinearity, a frequency domain ARX model is used. In a traditional time-series application, an ARX model attempts to predict response at the current time point based on its own past time point responses, as well as the current and past inputs to the system. A frequency domain ARX model attempts to predict the response at a particular frequency based on the input at that frequency, as well as responses at surrounding frequencies. The responses at the surrounding frequencies are included as inputs to the model to account for subharmonics and superharmonics introduced to the system through nonlinear feedback. More details on frequency domain analysis of data using an ARX model can be found in [10,11].

There are many possible forms of the frequency domain ARX model, with each depending on how the effects of subharmonics and superharmonics are to be considered. In this case, the effects of nonlinearities in the system are accounted for by using a first order model, which is the simplest model available. This first order ARX model in the frequency domain can be represented as follows:

$$\mathrm{Y}(k) = \mathrm{B}(k)\mathrm{U}(k) + \mathrm{A}_1(k)\mathrm{Y}(k - 1) + \mathrm{A}_{-1}(k)\mathrm{Y}(k + 1) \qquad k = 2, 3, \ldots, N_f - 1 \tag{2}$$

where N_f is the highest frequency value examined, Y(k) is the response at *kth* frequency, U(k) is the input at *kth* frequency, and Y(*k-1*) and Y(*k+1*) are the responses at (*k-1)th* and (*k+1)th* frequencies, respectively. $A_1(k)$ and $A_{-1}(k)$ are the frequency domain auto-regressive coefficients, and B(k) is the exogenous coefficient. The distinction of these two coefficients is important. While the exogenous coefficient describes the linear transmissibility effects, the auto-regressive coefficients describe any nonlinear effects that may be present in the system. In this study, Equation (2) is used to predict what the frequency response of one accelerometer will be given the frequency response of the second accelerometer at that joint. That is, one accelerometer response is treated as an input and the other accelerometer response is treated as an output. The features to be examined are the auto-regressive coefficients in this frequency domain transmissibility model. These coefficients are used as features to differentiate between damaged and undamaged conditions.

Because Y(k) and U(k) in Equation (2) are complex numbers, the B(k), $A_1(k)$ and $A_{-1}(k)$ coefficients are also complex. Therefore, for each frequency k there are 6 unknown coefficients that must be determined. In order to estimate the ARX coefficients, multiple sets of data need to be taken while the structure is in the same condition. All time history data are first standardized by subtracting the mean and dividing by the standard deviation, as in Equation (1). Because only three 4096-point time histories are available for each damage condition, each time history is divided into five separate 2048-point blocks, with 75% overlap. At this point, a Hanning window is applied to each block of data. A Fast Fourier Transform (FFT) is then performed on all data blocks in order to transfer the time history information into the frequency domain.

There are 15 equations (5 FFTs from each of the available three time histories) and 6 unknown coefficients, for each frequency value k, that must be solved. B(k), $A_1(k)$ and $A_{-1}(k)$ are then determined by minimizing the sum of the squared error associated with how well the model in Equation (2) describes the measured data. This process is done in the following way. If $\mathbf{y}(k)$ denotes the (*N x 1*) vector of output measurements at a particular frequency k,

$$\mathbf{y}^{\mathrm{T}}(k) = [\mathrm{Y}_1(k) \;\; \mathrm{Y}_2(k) \;\; \ldots \;\; \mathrm{Y}_N(k)] \qquad \textbf{(3)}$$

where N is the number of FFTs to be examined, $\mathbf{u}(k)$ denotes the (N *x 1*) vector of input measurements,

$$\mathbf{u}^{\mathrm{T}}(k) = [\mathrm{U}_1(k)\ \ \mathrm{U}_2(k)\ \ \ldots\ \ \mathrm{U}_N(k)] \tag{4}$$

and $\mathbf{p}$ denotes the (*3 x 1*) column vector of ARX coefficients,

$$\mathbf{p}^{\mathrm{T}}(k) = [\mathrm{A}_1(k)\ \ \mathrm{A}_{-1}(k)\ \ \mathrm{B}(k)] \tag{5}$$

then the error in the model for these samples is:

$$\mathbf{e}(k) = \mathbf{y}(k) - [\mathbf{y}(k-1)\ \ \mathbf{y}(k+1)\ \ \mathbf{u}(k)]\mathbf{p} = \mathbf{y}(k) - \mathbf{A}\mathbf{p} \tag{6}$$

The set of ARX coefficients that minimizes the sum of the squared error,

$$\sum_{i=1}^{N} \mathbf{e}_i^2(k) \tag{7}$$

across the N FFT samples, is selected by making the residual error vector, $\mathbf{y}(k) - \mathbf{A}\hat{\mathbf{p}}$, as nearly orthogonal as possible to the measured output data, $\mathbf{y}(k)$. $\hat{\mathbf{p}}$ is the estimate of $\mathbf{p}$, which is the true vector of ARX coefficients. The pseudoinverse of $\mathbf{A}$, denoted here as $\mathbf{A}^{+}$, produces the desired estimate:

$$\hat{\mathbf{p}} = \mathbf{A}^{+}\mathbf{y}(k) = (\mathbf{A}^{\mathrm{T}}\mathbf{A})^{-1}\mathbf{A}^{\mathrm{T}}\mathbf{y}(k) \tag{8}$$

This procedure is performed for every frequency value k. In this paper, variables displayed in bold indicate that a vector is being represented.

4) Statistical Model Development

Statistical model development is the area of SHM that is least developed to date. Very few of the available SHM techniques have incorporated algorithms that analyze the extracted features from the data and unambiguously determine the damage state of the structure. Examination of the aforementioned features using rigorous statistical procedures should yield information that allows a diagnosis of damage state in the monitored structure.

Because the information being sought is a measure of the nonlinearity of the data, the auto-regressive coefficients are used instead of the exogenous coefficient for analysis of the results. Because of symmetry in the ARX frequency domain model, only the $\mathbf{A}_1(k)$ coefficients are considered for damage detection. The

feature that is statistically analyzed is the difference between the auto-regressive coefficients of a known undamaged state, $\mathbf{A}_1^{u}(k)$, and the coefficients from a state that is to be determined, $\mathbf{A}_1^{d}(k)$. Damage in the structure causes the auto-regressive coefficients to differ from the undamaged coefficients at various frequencies. Certain frequencies are more sensitive to damage in the joint and cause a greater difference between auto-regressive coefficients than other frequencies. Therefore, the extracted feature will be at a maximum (or a minimum) at these certain frequencies. This observation shows that the most useful data for identifying damage to the structure will come in the tails of the feature distribution.

If this new feature of the auto-regressive coefficient difference, which will now be referred to as **G**(*k*), has a Gaussian distribution, then a standard control chart [12] could be applied to monitor the status of the system. However, by plotting the feature on a normal probability chart, shown in Figure 4, it is revealed that the tails of the distribution deviate significantly from the normal distribution. If the data in Figure 4 were normally distributed, they would plot as a straight line. The normal probability chart clearly indicates that the data are not normally distributed near the tails, and therefore any control chart based on a normality assumption of the data will show an inflated number of outliers for a given confidence limit. These extra outliers can lead to a false positive indication of damage. The extra outliers will be a result of the tails of the actual distribution being much longer than that of the normal distribution. This result can be seen in Figure 5. The non-Gaussian nature of the data suggests that a different method of statistical analysis should be used.

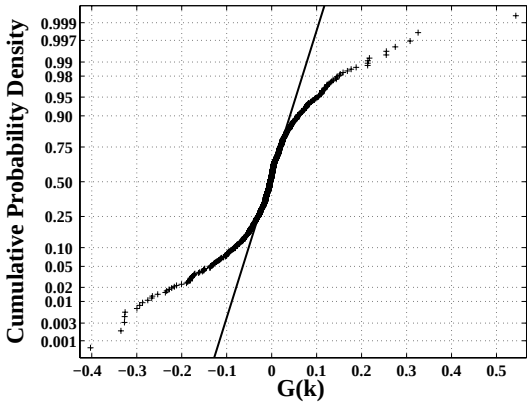

Figure 4: Normal probability plot of the feature **G**(*k*)

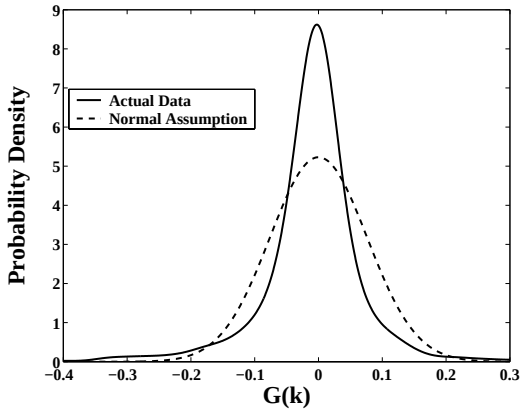

Figure 5: Probability density function of the extracted feature **G**(*k*) vs. the normality assumption

EVS is used in this analysis to accurately model the behavior of the feature distribution's tails. The basis of this branch of statistics stems from the following situation. If a moving window is taken along a vector of samples and the maximum value is independently selected from each of these windows, the induced cumulative density function of the maxima of the samples, as the number of vector samples tends to infinity, asymptotically converges to one of three possible distributions: Gumbel, Weibull, or Frechet [13].

$$\text{Gumbel: } F(x) = \exp\left[-\exp\left(\frac{\lambda - x}{\delta}\right)\right] \quad -\infty < x < \infty \text{ and } \delta > 0 \tag{9}$$

$$\text{Weibull: } F(x) = \begin{cases} 1 & \text{If } x \geq \lambda \\ \exp\left[-\left(\frac{\lambda - x}{\delta}\right)^{\beta}\right] & \text{otherwise} \end{cases} \tag{10}$$

$$\text{Frechet: } F(x) = \begin{cases} \exp\left[-\left(\frac{\delta}{x - \lambda}\right)^{\beta}\right] & \text{If } x \geq \lambda \\ 0 & \text{otherwise} \end{cases} \tag{11}$$

where λ, δ and β are the model parameters that are estimated from the data. Similarly, there are only the same three types of distributions for minima.

The appropriate distribution is chosen by plotting the extracted vector of maxima on the probability paper for a Gumbel distribution. The vector will plot in a linear fashion if it has a Gumbel maximum distribution. Otherwise, the vector will have an associated curvature. If this curvature is concave, the feature vector has a Weibull maximum distribution. Similarly, if the curvature is convex the feature vector has a Frechet maximum distribution. Model parameters are then estimated by fitting the chosen distribution to the data. For the Frechet and Weibull distributions, the location parameter λ must be estimated *a priori* to computing the δ and β parameters. While there are analytical approaches that can estimate the location parameter, in this study it was chosen by using an initial guess based on the parameter's limits with respect to the maximum

data. The final value was then chosen by varying the initial guess until the maxima vector plotted as linearly as possible on probability paper for the chosen maximum distribution (See Figure 6).

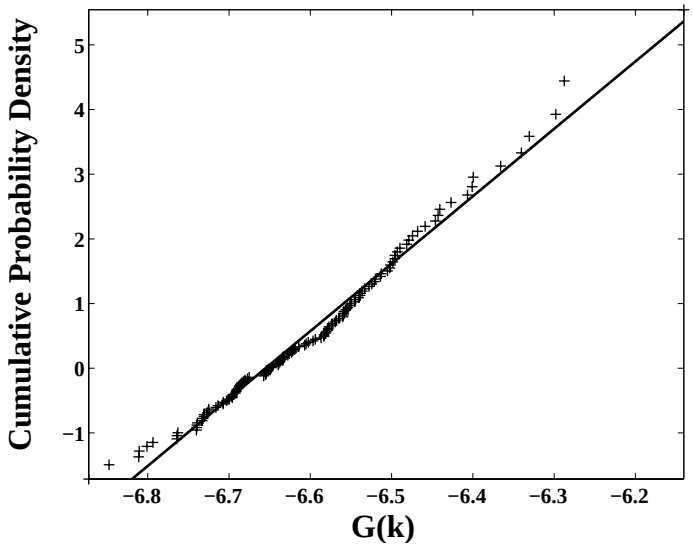

Figure 6: Probability plot for **G**(*k*) shown on Frechet probability paper

Once the model parameters are chosen, it is possible to generate confidence limits that can be applied to the distribution. These limits are far more accurate than those obtained when assuming a Gaussian distribution. The thresholds corresponding to a specific confidence level are given by the following equations [14]:

$$\text{Gumbel: } x_{max} = \lambda - \delta \ln\left[-\ln\left(1-\frac{n\alpha}{2}\right)\right] \quad \textbf{(12)}$$

$$\text{Weibull: } x_{max} = \lambda - \delta \ln\left[-\ln\left(1-\frac{n\alpha}{2}\right)\right]^{\frac{1}{\beta}} \quad \textbf{(13)}$$

$$\text{Frechet: } x_{max} = \lambda + \frac{\delta}{\left[-\ln\left(1-\frac{n\alpha}{2}\right)\right]^{\frac{1}{\beta}}} \quad \textbf{(14)}$$

where n is the window size used to extract the maxima, and α is the associated Type I error of the confidence limit. Type I error is simply the percentage of false positives that are expected to appear. For

example, when using a 95% confidence interval the Type I error is expected to be 5% ($\alpha = 0.05$). It should be noted that the upper confidence limit is calculated from the associated maxima distribution and the lower confidence limit is calculated from the associated minima distribution. For simplicity, only the maxima distribution and upper confidence limit are mentioned in the analysis procedure. However, minima distribution and the lower confidence limit can be readily found in a similar manner.

After a FFT is applied to the sample block length of 2048 points, the sample length is reduced to 1024 points in the frequency domain. Of these points, only the first 800 points are used, to disregard the effect of a leakage problem at the high frequency range. Therefore, the distribution of **G**(k) has 800 data points. A window of 10 samples is moved along the parent vector and the maximum of each window is then extracted. This process generates a maxima vector of 80 points to be analyzed by EVS. Once a distribution is chosen, the model parameters must be estimated. Only a portion of the data points in the maxima vector are used to compare to the fitted model, because agreement with the upper end of the extracted maxima vector is more important than agreement with the entire vector. An example of this result can be seen in Figure 7, which shows an acceptable fit of maxima in a Frechet distribution.

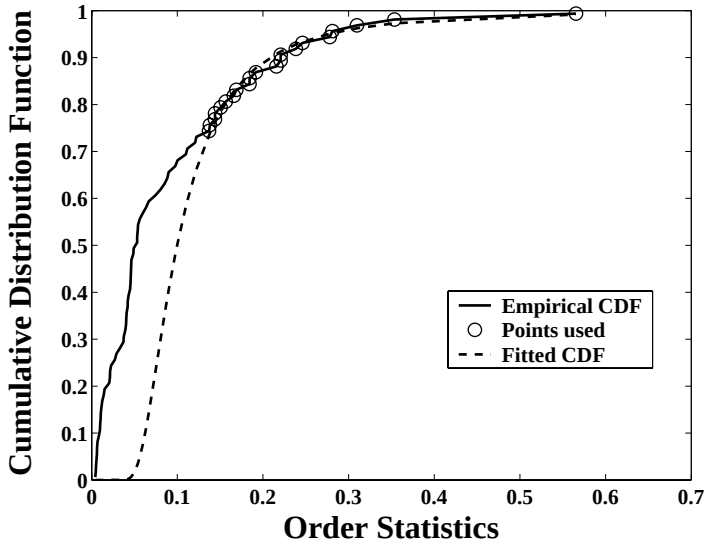

Figure 7: Curve fit for Frechet maxima distribution

2.3 Results

Five sets of data are used for the analysis of each damage case. The first set is the baseline undamaged data that are used to set the confidence limits. These limits are tested against data sets from all three damage levels (1.8 N-m, 0.6 N-m, and no bolts) and against another undamaged case to be sure that false positives do not occur. For all cases, it is determined that the Frechet distribution, for both maxima and minima, is the most appropriate extreme value distribution to use for the analysis. After the location parameter, λ, is estimated through trial-and-error, the other model parameters are found by fitting the parametric model to the extracted maximum and minimum data. The upper and lower confidence limits corresponding to a 99.5% confidence interval ($\alpha = 0.005$) are then calculated from the known parameters using Equation (14), or an equivalent equation for minima.

Previous work has shown that the application of the EVS-based statistical model shows excellent results when applied to a joint in the structure that is known to be damaged [15]. Table 2 compares the effectiveness of the limits found using EVS with those calculated based on the normality assumption of the data. All numbers displayed in parentheses are associated with the normality assumption. For a sample size of 800 points and a 99.5% confidence interval, one should expect 2 outliers on each side of the confidence interval for undamaged data.

Table 2: Number of outliers estimated by EVS for particular damage case at a damaged joint

Damage Level	Lower outliers	Upper outliers
Baseline	1 (15)*	1 (10)
Undamaged	2 (11)	0 (12)
1.8 N-m preload	88 (166)	20 (64)
0.6 N-m preload	110 (202)	28 (79)
Bolts removed	9 (30)	38 (111)

* Results from the normality assumption are shown in parentheses.

Clearly, the confidence limits derived for the undamaged case using EVS are much closer to the actual 99.5% limits than those derived using the normality assumption. Note that there is a significant drop in the number of outliers for the most severe damage level in which the bolts are completely removed from the structure.

This result is most likely because the damage detection scheme is based on the modeling of the nonlinear system input/output relationship. When the bolts are completely removed, the source of local nonlinearity (the loose bolts rattling against the plate) disappeared. This causes the number of outliers detected using the EVS confidence limits to drastically drop when compared to the other damage cases.

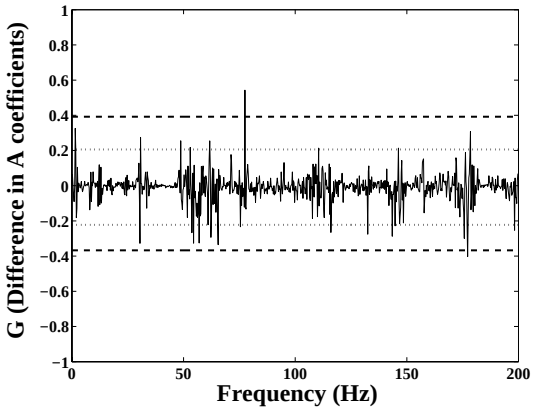

Figure 8: 99.5% Confidence Interval of baseline undamaged case with legend (solid line: **G**(k), dashed outer lines: EVS confidence limit, dotted inner lines: normal confidence limit)

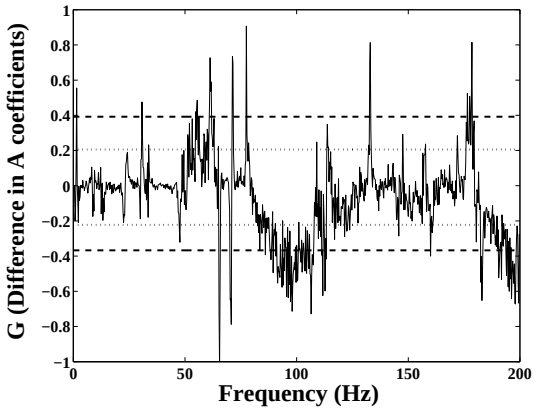

Figure 9: 99.5% Confidence Interval of 1.8 N-m damage case with legend (solid line: **G**(k), dashed outer lines: EVS confidence limit, dotted inner lines: normal confidence limit)

Figures 8 and 9 show plots of data and both EVS and normal confidence limits for the baseline undamaged condition and the 1.8 N-m damage level. Figure 8 shows only one outlier on each side of the EVS confidence interval. This result is slightly less than the expected outcome of two outliers on each side. However, this EVS confidence interval does not produce a false positive result, so it is considered acceptable. It is clear that if confidence limits based upon the normality assumption are used, there are many false positives, which negates any usefulness that the analysis method sought. Quantitatively, there are approximately six times as many outliers as should be present with a 99.5% confidence interval, as seen in Table 2 for the baseline condition. Figure 9 shows the effectiveness of using auto-regressive coefficients from the frequency domain ARX model to detect damage. There is a clear graphical aberration of the test data from the data taken during the undamaged state. Both the EVS and normal confidence limits correctly indicate damage has taken place.

Several damage cases were fully analyzed by examining data from each of the 12 instrumented joints on the test structure. Results from two damage cases that best show the effectiveness of this method are shown here. The first set of data comes from damage case 1 in which joint 2a, which is on the corner farthest from the shaker on third (highest) floor of the test structure, is the damaged joint. In this case, the base excitation is at the high RMS level of 1 V. The results of the aforementioned damage detection scheme can be seen in Table 3. Again, the expected number of outliers for an undamaged joint is 4 when 99.5% confidence limits are established. Results from the undamaged condition are mostly positive, with only joint 1c showing an inflated number of outliers. While the method appears to have failed to properly classify the undamaged case of joint 1c because of the large number of outliers, a graphical inspection of the test feature $\mathbf{G}(k)$ along with the EVS confidence limits shows that 5 of the 9 outliers are barely outside the established confidence limit. Such results would be less likely to occur with a larger amount of baseline data to establish the EVS confidence limits. The results would also benefit from a more rigorous optimization protocol for choosing the EVS parameters. Research is underway to solve a nonlinear optimization problem to simultaneous optimize these parameters.

Table 3: Total number of outliers using EVS confidence limits for increasing damage levels under the high level (1 V) of base excitation. The shaded region indicates the damaged joint in the structure.

Damage Level	Joints											
	1st Floor				2nd Floor				3rd Floor			
	1c	2c	3c	4c	1b	2b	3b	4b	1a	2a	3a	4a
Undamaged*	9	4	3	2	2	4	4	2	2	2	3	3
1.8 N-m damage	16	27	38	18	15	12	18	15	32	58	35	22
0.6 N-m damage	25	30	38	17	16	16	19	16	40	90	31	23
No bolt damage	34	28	37	23	24	17	21	28	39	25	33	24

* Nominal preload value of 25 N-m

The damage cases, however, show that the damage detection scheme is unable to localize damage and causes all joints in the test structure to appear damaged according to the number of outliers in Table 3. For the damage levels in which the bolts are not removed from the structure, the joint at which the damage was induced showed the largest number of outliers. This observation suggests that the proposed method might be

able to locate the damaged joint. However, for cases in which multiple joints in the building are damaged, choosing the joint with the highest number of outliers as the only damaged joint would not produce a correct result. In addition, by examining the damage level in which the bolt is completely removed, it can be seen that many other joints in the building actually produce more outliers than the damaged joint.

The second set of data comes from damage case 2 where joint 4b, which is on the corner directly above the shaker on the second (middle) floor of the test structure, is the damaged joint. In this case, the base excitation is at the low RMS level of 0.25 V. The results can be seen in Table 4. The undamaged condition shows somewhat worse results than in the first case. However, as previously stated, the inflated number of outliers for the undamaged condition is not a sign that the damage detection scheme has failed to distinguish between damaged and undamaged cases.

Table 4: Total number of outliers using EVS confidence limits for increasing damage levels under the low level (0.25 V) of base excitation. The shaded region indicates the damaged joint in the structure.

Damage Level	Joints											
	1st Floor				2nd Floor				3rd Floor			
	1c	2c	3c	4c	1b	2b	3b	4b	1a	2a	3a	4a
Undamaged*	3	6	4	3	9	3	4	4	4	8	10	4
1.8 N-m damage	13	14	24	31	24	40	22	24	28	19	29	21
0.6 N-m damage	11	15	31	33	23	39	25	22	32	20	27	18
No bolt damage	18	15	28	29	42	53	27	35	40	25	44	33

* Nominal preload value of 25 N-m

Examination of the damage cases leads to similar conclusions. The results are not as good as with the high excitation, as the numbers of outliers from the damaged joint are never the highest of all joints. In particular, joint 2b has the highest number of outliers for all damage levels but is not the damaged joint. The low number of outliers for the damage levels where the bolts are still present is most likely caused by the inability of the low excitation level, and the shaker frequency range being used, to excite the local nonlinearity in the damaged joint. The inconsistency between results from the high excitation level and the low excitation level indicates that a high excitation level is required to produce nonlinear responses. In addition, the inability of

the current method to localize damage within the structure indicates that a new method must be undertaken to address this vulnerability. These deficiencies in the vibration-based scheme led to the development of the following impedance-based method.

3. IMPEDANCE-BASED METHOD

3.1 Theory and Background

Piezoceramic transducers acting in the "direct" manner produce an electrical charge when mechanically deformed. Conversely, a mechanical strain is produced when an electrical field is applied to the transducer. The process to be used with the impedance-based monitoring technique uses both the direct and converse version of the piezoelectric effect simultaneously to obtain an impedance signature for the structure. A PZT patch is first bonded to the structure with a high-strength adhesive to ensure strong mechanical interaction. When this PZT patch is driven by a fixed, alternating electric field, a small deformation is produced in the PZT wafer, which in turn provides an input to the attached structure. The subsequent response to the mechanical vibration is transferred back to the PZT wafer in the form of an electrical response (See Figure 10). When damage causes the mechanical dynamic response to change, it is manifested in the electrical response of the PZT wafer. The electrical impedance, which is the ratio of the input voltage to the output current, is coupled with the structural impedance through the following equation [16]:

$$\frac{1}{Z_p(\omega)} = i\omega a\left(\bar{\varepsilon}_{33}^{T}(1 - i\delta) - \frac{Z_s(\omega)}{Z_s(\omega)+Z_a(\omega)} d_{3x}^2 \hat{Y}_{xx}^{E}\right) \quad \textbf{(15)}$$

where Z_p is the electrical impedance of the PZT, Z_a and Z_s are the mechanical impedances of the PZT material and structure, respectively, Y_{xx}^{E} is the complex Young's modulus of the PZT with zero electric field, d_{3x} is a PZT coupling constant in the arbitrary x-direction at zero stress, $\bar{\varepsilon}_{33}^{T}$ is a dielectric constant at zero stress, δ is the dielectric loss tangent of the PZT, and *a* is a geometric constant of the PZT. When a structure becomes damaged, the mechanical impedance is altered by changes in the structural stiffness and/or damping.

Because all other variables in Equation 15 are determined only by the PZT properties, only the external structure's impedance, Z_s, uniquely determines the overall electrical impedance of the PZT. Therefore, a

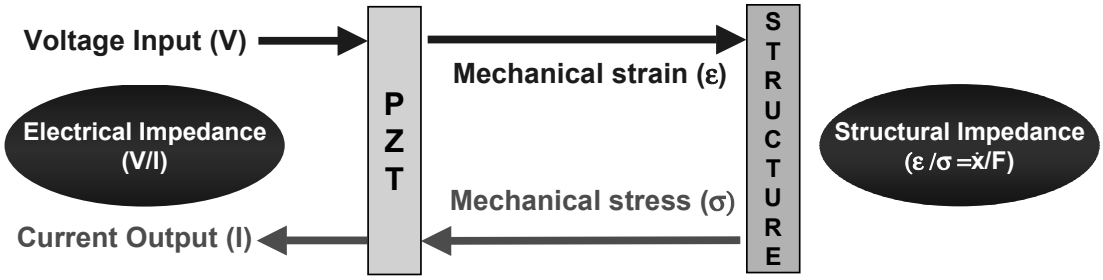

Figure 10: Diagram of impedance-based SHM method

frequency domain ARX model and the voltage output from the PZT circuit, as seen in Figure 11, is used as the input. These voltages are measured in the time domain, which is different from the traditional impedance-based methods that only record data in the frequency domain. V_{out} is proportional to the output current of the PZT. The electrical impedance of the PZT patch is related to the measured voltage in and voltage out of the PZT through the following equation:

$$Z_p = \frac{V_p}{I_p} = \frac{V_{in} - V_{out}}{V_{out}/R} = R\left(\frac{V_{in}}{V_{out}} - 1\right) \quad \textbf{(16)}$$

Again, the difference in $\mathbf{A}_1(k)$ coefficients determined by the ARX model is used, along with EVS, to determine the damage state of each joint. The use of EVS with the impedance-based method is important

because there are currently no limits framed in a rigorous statistical manner that have been used with this method. It should also be noted that previous impedance-based methods were required to implement a compensation technique for vertical and horizontal shifting of the impedance measurements that take place because of temperature and other normal variations. This technique is able to avoid this step because these shifts are completely characterized by the $\mathbf{B}(k)$ coefficients and do not affect the $\mathbf{A}_{1,-1}(k)$ coefficients. This result adds another level of robustness of the frequency domain ARX model to natural variations of the system.

PZT.bmp (400x454x16M bmp)

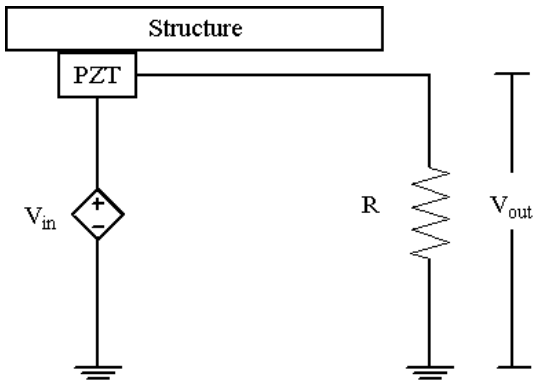

Figure 11: Diagram of PZT circuit indicating locations of measured voltages V_{in} and V_{out}

3.2 Experimental Setup

The same three-story structure used for the previous vibration-based analysis is used in this test setup (Figures 1, 2 and 3). No accelerometers are mounted on the structure. Instead, four PZT patches (2.5 cm x 2.5 cm x 0.025 cm) are bonded to the brackets that affix the second, or middle, floor to the unistrut columns (Figure 12). Only one floor was instrumented because of hardware limitations. However, damage initiated on one floor should not affect the impedance measurements of joints on other floors because of the design of the test structure. The voltage signal into the PZT patch has a frequency content of 0-20 kHz and a peak voltage of 5 V. Note that the power necessary to create the input signal is relatively low because the current is only 4.7 mA. A “healthy” joint, in this case, is held together by bolts that are torqued to a value of 28 N-m. Damage is introduced by completely removing the preload (0 N-m) of one of the bolts attaching the plate to the bracket, as seen in Figure 12.

Figure 12: Close-up of a joint with bonded PZT patch (light circle) and loosened bolt in damage case (dark circle)

An impedance analyzer that can measure up to 10 MHz in the frequency domain is normally used for impedance-based damage detection. However, the method proposed in this paper requires data in the time domain and the conventional impedance analyzer cannot be used. Therefore, a data acquisition system that samples at 48 kHz in the time domain (20 kHz in the frequency domain after anti-aliasing) is used, producing 32,768 time points. Three time histories are recorded for each of the four instrumented joints while they are in the undamaged condition. Damage case 1 is then implemented by completely loosening one bolt at joint 4b. One time history for each joint is recorded with the structure in this condition. Damage case 2 is then created by loosening one of the bolts at joint 2b while the bolt at joint 4b remains loose. Again, one time history is recorded for each joint with the structure in this condition. Damage case 2 is intended to study the effects of multiple damage locations. The structure has no base excitation input, for reasons explained in Section 3.3. A commercial data acquisition system controlled from a laptop PC is used to digitize the voltage analog signals.

The original length of the voltage time signals is 32,768 points. Using blocks of 4096 points with 75% overlap reduces the sample length to 4096 points. Applying a FFT to each block further reduces the sample length to 2048 points in the frequency domain. As before, a Hanning window is applied to each data block before the FFT is performed. Of these points, only those corresponding to the frequency range of 5-20 kHz

are kept because of anti-aliasing techniques used above 20 kHz and the inability of the PZT patch to sufficiently excite the structure below 5 kHz. Based on this frequency range, voltage input into the structure is limited to 0-20 kHz. This leaves the distribution of **G**(k) with 1280 data points. A window of 10 samples is moved along the parent vector and the maximum of each window is then extracted. This process generates a maxima vector of 128 points to be analyzed by EVS. A 99.5% confidence interval is used to set up confidence limits for each joint by constructing a vector **G**(k) that is the difference between the first two undamaged cases. The first undamaged case is used as the baseline measurement for all joints. The third undamaged case is used as a false positive test.

3.3 Operational Variation

Before initiating the above experiment, a study was done to verify that the impedance-based method is insensitive to arbitrary ambient inputs to the structure. This procedure is important because civil infrastructure, such as buildings and bridges, have various ambient excitation sources including wind loading, traffic, and temperature variation. The features extracted for damage detection need to be insensitive to these normal variations to minimize false indications of damage. The real part of the impedance measurement was examined from 40-50 kHz using the impedance analyzer while a variety of base excitation input waveforms, including background noise (baseline), burst random, sine chirp, impulse, random, sine, and white noise, were used as disturbances to simulate operational variation. The frequency content of these waveforms varied, but at most was as high as 10 kHz. Damage was then initiated by loosening one bolt that attaches the plate to the column at joint 4b. Figure 13 shows that variations in the impedance measurement between different input waveforms are negligible, especially when compared to the impedance change caused by damage. Therefore, the impedance-based method succeeds in addressing one of the major vulnerabilities of the vibration-based method because it is insensitive to ambient vibration. Again, it should be noted that the examined frequency range is above the 5-20 kHz that is used for the damage detection scheme because the impedance analyzer is able to measure very high frequencies.

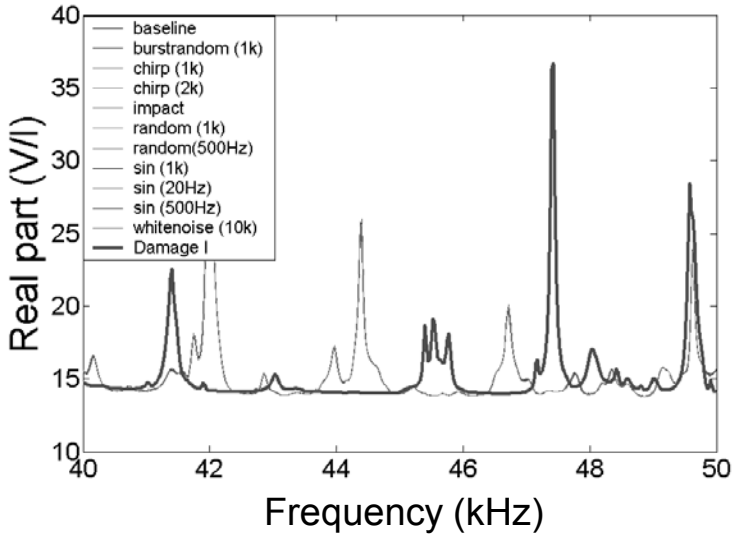

Figure 13: Insensitivity of electrical impedance to various base excitation input waveforms vs. sensitivity of electrical impedance to damage

3.4 Results

Four sets of data are used in each analysis. The first set is the baseline undamaged data that are used to set the confidence limits. These limits are tested against data sets from an alternate undamaged case as well as the two previously described damage cases. A normality check, similar to Figure 4, showed that the data were not normally distributed in the tails. For all joints it was determined that the Frechet distribution, for both maxima and minima, was the most appropriate extreme value distribution to use for the analysis. For a sample size of 1280 points and a 99.5% confidence interval, one should expect 6 outliers beyond the confidence interval for the undamaged cases.

Figures 14 and 15 show $\mathbf{G}(k)$, as well as the associated 99.5% confidence interval, for joint 4b. Figure 14 depicts the baseline undamaged case and Figure 15 shows damage case 1, in which the preload of one bolt at joint 4b is removed. There is a clear visual distinction between the undamaged and damaged conditions. Of particular note is the fact that the 15-20 kHz range, in Figure 15, is more sensitive to damage than the lower examined frequencies. Therefore, examining a higher frequency range has several benefits, including increased damage sensitivity and better damage localization. This result was expected, and higher frequency ranges (> 30 kHz) would have been used if not for current hardware limitations. With a frequency range of 0-

20 kHz, it is expected that damage initiated at one joint will be picked up by PZT sensors at the other joints. However, the number of outliers should be able to predict the location of the damaged joint, unlike the previous vibration-based analysis.

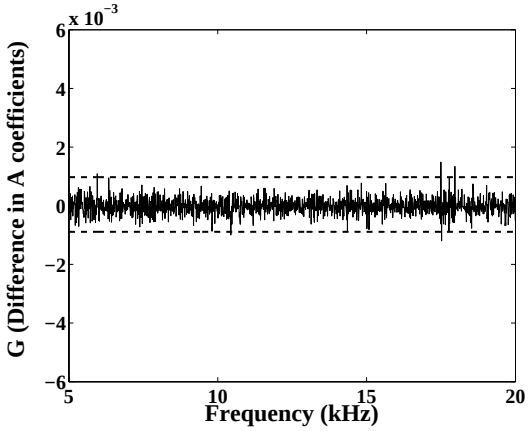

Figure 14: 99.5% Confidence Interval of baseline undamaged case for joint 4b with legend (solid line: **G**(k), dashed lines: EVS confidence limit)

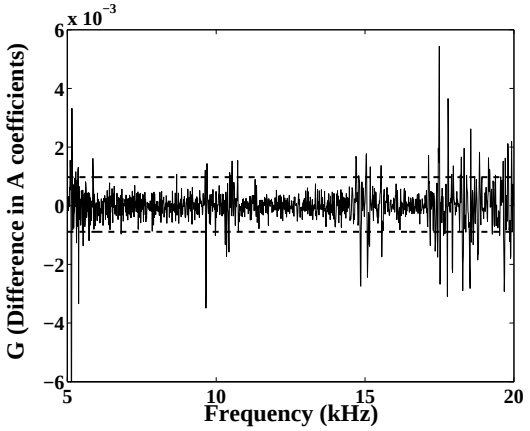

Figure 15: 99.5% Confidence Interval of damage case 1 for joint 4b (damaged) with legend (solid line: **G**(k), dashed lines: EVS confidence limit)

Table 5: Total number of outliers using EVS confidence limits for each joint. For each case, the shaded region indicates the damaged joint(s) in the structure.

Damage Cases	Joint			
	1b	2b	3b	4b
Baseline	7	9	7	5
Undamaged	10	10	10	8
Damage case 1	40	37	50	115
Damage case 2	75	115	72	133

To examine the results, the number of outliers for each joint and for each examined damage case is shown in Table 5. Examination of these numbers shows excellent results for this damage detection technique. Again, 6 outliers are expected for an undamaged case. However, any number of outliers that is close to this number should be considered undamaged because the established confidence limits are still not the true confidence limits. Therefore, all undamaged cases are diagnosed as undamaged by the damage detection scheme. Damage case 1 shows a large increase in the number of outliers for joint 4b (the damaged joint) and small increases in the number of outliers for the other joints. This outcome is exactly what was expected due to

examination of the low frequency range of 5-20 kHz, in relation to the normal impedance range of greater than 30 kHz. Damage case 2 has multiple damage locations at joints 4b and 2b. A very small increase in the number of outliers at joint 4b shows that the diagonal distance between joints 4b and 2b is on the edge of the sensing range of the impedance-based method when using the low frequency range. On a real world structure, sensors that are able to measure very high frequencies may not be necessary because joints are a much larger distance apart. Again, there is a large jump in the number of outliers at the newly damaged joint and a small jump in the number of outliers and joints 1b and 3b. This result shows that the impedance-based method can also detect multiple damage locations.

4. SUMMARY

Auto-regressive coefficients from a frequency domain ARX model show promise as a powerful feature for nonlinear damage discrimination. The addition of EVS as a means for establishing confidence limits greatly enhances this damage classification technique. Unfortunately, the vibration-based method is unable to localize damage in the test structure to a particular joint and fails to address the data normalization issue. The integration of the impedance-based active sensing method into the frequency domain ARX model, however, shows very promising results with regard to damage localization and data normalization. While the data acquisition system that is used requires the frequency range examined by the frequency domain ARX model to be below the usual range used for impedance measurements, the results still indicate a clear difference between damaged and undamaged joints.

There are several unique aspects of this study. The explicit consideration of nonlinear features extracted from the data makes this technique better able to identify damage that causes nonlinear response of the structure. The inclusion of EVS improves the reliability of the method by placing it within a rigorous statistical framework. In addition, many damage detection schemes require data from a structure in both undamaged and damaged conditions to set up decision limits. Using EVS, this method only needs data from the

undamaged condition to set up proper confidence limits. Initial measurement of impedance signals in the time domain is also a unique aspect of the proposed damage detection method.

Future work should involve a study of damage localization using the impedance-based method at higher frequencies, once the necessary sensing equipment becomes available. It is hoped that the ability of the ARX model to examine nonlinearities within the structure as well as the rigorous statistical boundaries found through the application of EVS will result in a damage detection scheme that is able to localize damage within the structure without producing any false positive results.

The path forward for this damage detection scheme is to embed the program into an on-board microprocessor that can be distributed on critical joints of a moment-resisting frame structure in a seismic region. This onboard microprocessor will have the ability to be self-powering (likely through the use of ambient vibration of the structure) [18]. The microprocessor will also be able to communicate with a central computer system that will monitor the results from all the sensors distributed throughout the building [19]. Although the PZT patches and microprocessors would be distributed throughout the structure, the cost of such a system would be substantially less than a system based on PZT accelerometers. The central computer system would be able to quantify the existence of damage through a process that is quick and easy to automate. Such a system would constitute a tremendous benefit for both life safety and economic concerns.

ACKNOWLEDGEMENT

Funding for this project was provided by the Department of Energy through the internal funding program at Los Alamos National Laboratory known as Laboratory Directed Research and Development (8M05-X1MV-0000-0000). The authors acknowledge Tim Johnson and Seth Gregg and the Los Alamos Dynamic Summer School for providing the test structure as well as helping with the set-up, instrumentation and acquisition of data from the test structure. Funding for the summer school was provided by the Engineering Sciences and Application Division at Los Alamos National Laboratory and the Department of Energy's Education Program Office.

REFERENCES

1. Steel Moment Frames After Northridge. *Special Issue of the Journal of Structural Engineering* 2000. Darwin D, Editor; **126**(1).
2. Bray D, McBride D. *Nondestructive Testing Techniques*; John Wiley & Sons: New York, 1992.
3. Doebling SW, Farrar CR, Prime MB. A Summary Review of Vibration-Based Damage Identification Methods. *Shock and Vibration Digest* 1998; **30**(2):91-105.
4. Sohn H, Farrar CR, Hemez FM, Czarnecki JJ, Shunk DD, Stinemates DW, Nadler BR, "A Review of Structural Health Monitoring Literature: 1996-2001," Los Alamos National Laboratory Report, LA-13976-MS, 2004.
5. Adams DE, Allemang RJ. Discrete Frequency Models: A New Approach to Temporal Analysis. *ASME Journal of Vibration and Acoustics* 2000; **123**:98-103.
6. Park G, Cudney H, Inman DJ. Impedance-Based Health Monitoring of Civil Structural Components. *Journal of Infrastructure Systems* 2000; **6**(4):153-160.
7. Farrar CR, Stinemates DW, Hemez FM, Sohn H, "Structural Health Monitoring Design Using Finite Element Analysis," *SPIE's 7th Annual International Symposium on NDE for Health Monitoring and Diagnostics,* San Diego, CA, March 17-21, 2002.
8. Fasel TR, Gregg SW, Johnson TJ, Farrar CR, Sohn H. Experimental Modal Analysis and Damage Detection in a Simulated Three Story Building. *Proceedings of the 20th International Modal Analysis Conference*; Los Angeles, CA, 2002.
9. Farrar CR, Doebling SW, Nix DA. Vibration-Based Structural Damage Identification. *Philosophical Transactions of the Royal Society: Mathematical, Physical & Engineering Sciences* 2001; **359**(1778):131-149.
10. Adams DE. Frequency Domain ARX Models and Multi-Harmonic FRF Estimators for Nonlinear Dynamic Systems. *Journal of Sound and Vibration* 2001; **250**(5):935-950.
11. Adams DE, Farrar CR. Identifying Linear and Nonlinear Damage Using Frequency Domain ARX Models. *International Journal of Structural Health Monitoring* 2002; **1**(2):185-201.

12. Sohn H, Czarnecki JJ, Farrar CR. Structural Health Monitoring Using Statistical Process Control. *Journal of Structural Engineering* 2000; **126**(11):1356-1363.
13. Castillo E. *Extreme Value Theory in Engineering*; Academic Press Series in Statistical Modeling and Decision Science: San Diego, CA, 1988.
14. Worden K, Allen DW, Sohn H, Stinemates DW, Farrar CR. Extreme Value Statistics for Damage Detection in Mechanical Structures. *Los Alamos National Laboratory Report* 2002; LA-13903-MS.
15. Fasel TR, Sohn H, Farrar CR. Damage Detection Using Frequency Domain ARX Models and Extreme Value Statistics. *Proceedings of the 21st International Modal Analysis Conference*; Kissimmee, FL, 2003.
16. Liang C, Sun F, Rogers CA. Coupled Electromechanical Analysis of Adaptive Material System: Determination of Actuator Power Consumption and System Energy Transfer. *Journal of Intelligent Material Systems and Structures* 1994; **5**:12-20.
17. Park G, Sohn H, Farrar CR, Inman DJ. Overview of Piezoelectric Impedance-Based Health Monitoring and Path Forward. *Shock and Vibration Digest* 2003; in press.
18. Sodano H, Magliula EA, Park G, Inman DJ. Electric Power Generation Using Piezoelectric Devices. *Proceedings of the 13th International Conference on Adaptive Structures and Technologies*; Berlin, Germany, 2002.
19. Tanner NA, Wait JR, Farrar CR, Sohn H. Structural Health Monitoring Using Wireless Sensing Systems with Embedded Processing. *Journal of Intelligent Material Systems and Structures* 2003; in press.